

A micro-structured aperture made of a hollow triangular-core fiber for novel beam shaping

Woosung Ha,¹ Sejin Lee,¹ Jongki Kim,¹ Yoonseob Jeong,¹ Kyunghwan Oh,^{1,*}
Jens Kobelke,² Kay Schuster,² Sonja Unger,² Anka Schwuchow,² and Jun Ki Kim³

¹*Institute of Physics and Applied Physics, Yonsei University, 262 Seongsanno, Seodaemun-gu, Seoul 120-749, Korea*

²*Institute of Photonic Technology, Albert-Einstein St. 9, 07745 Jena, Germany*

³*Harvard Medical School and Wellman Center for Photomedicine, Massachusetts General Hospital, 40 Blossom St. BAR 812, Boston, MA 02114, USA*

*koh@yonsei.ac.kr

Abstract: We demonstrate a micro-structured aperture made of a unique hollow triangular-core fiber (HTCF) that consists of a central air hole, a high-index hollow triangular core, and silica cladding for all-fiber novel beam shaping. Detailed fabrication processes to embed a hollow triangular structure into a cylindrical optical fiber are described and unique diffraction patterns out of the HTCF for monochromatic light are analyzed both experimentally and theoretically. Fourier-optic analysis combined with guided mode calculation was pursued to interpret experimental patterns in terms of the beam propagation distance.

©2010 Optical Society of America

OCIS codes: (060.2270) Fiber characterization; (060.2280) Fiber design and fabrication; (060.2300) Fiber measurements; (060.2310) Fiber optics; (060.2400) Fiber properties.

References and links

1. F. M. Dickey, "Laser beam shaping," *Opt. Photon. News* **14**(4), 30–35 (2003).
2. J. W. Goodman, *Introduction to Fourier Optics*, 3rd ed. (Roberts and Company Publishers, Greenwood Village, CO, 2005).
3. M. Gu, and X. S. Gan, "Fresnel diffraction by circular and serrated apertures illuminated with an ultrashort pulsed-laser beam," *J. Opt. Soc. Am. A* **13**(4), 771–778 (1996).
4. L. J. Hornbeck, "Digital Light Processing for high-brightness, high-resolution applications," *Proc. SPIE* **3013**, 27–40 (1997).
5. H. Schenk, P. Dürr, T. Haase, D. Kunze, U. Sobe, H. Lakner, and H. Kück, "Large deflection micromechanical scanning mirrors for linear scans and pattern generation," *IEEE J. Sel. Top. Quantum Electron.* **6**(5), 715–722 (2000).
6. M. L. Huebschman, B. Munjuluri, and H. R. Garner, "Dynamic holographic 3-D image projection," *Opt. Express* **11**(5), 437–445 (2003), <http://www.opticsinfobase.org/oe/abstract.cfm?uri=oe-11-5-437>.
7. P. St. J. Russell, "Photonic-crystal fibers," *J. Lightwave Technol.* **24**(12), 4729–4749 (2006).
8. K. Oh, S. Choi, Y. Jung, and J. W. Lee, "Novel hollow optical fibers and their applications in photonic devices for optical communications," *J. Lightwave Technol.* **23**(2), 524–532 (2005).
9. J. K. Kim, J. Kim, Y. Jung, W. Ha, Y. S. Jeong, S. Lee, A. Tünnermann, and K. Oh, "Compact all-fiber Bessel beam generator based on hollow optical fiber combined with a hybrid polymer fiber lens," *Opt. Lett.* **34**(19), 2973–2975 (2009).
10. A. R. Tynes, A. D. Pearson, and D. L. Bisbee, "Loss mechanisms and measurements in clad glass fibers and bulk glass," *J. Opt. Soc. Am.* **61**(2), 143–153 (1971).
11. R. B. Dyott, C. R. Day, and M. C. Brain, "Glass-fibre waveguide with a triangular core," *Electron. Lett.* **9**(13), 288–290 (1973).
12. A. R. Tynes, "Partially clad triangular-cored glass optical fibers and lasers," *J. Opt. Soc. Am.* **64**(11), 1415–1423 (1974).
13. K. Oh, W. Ha, S. Lee, J. Kim, Y. Jeong, and M. Park, "Preforms for preparing polygonal-core optical fiber and preparation method thereof," Korean patent application 10–2010–0066761 (12 July 2010).
14. Heraeus website, <http://optics.heraeus-quarzglas.com>.
15. S. Choi, K. Oh, W. Shin, and U. C. Ryu, "Low loss mode converter based on adiabatically tapered hollow optical fibre," *Electron. Lett.* **37**(13), 823–825 (2001).
16. W. Ha, S. Lee, Y. Jung, J. K. Kim, and K. Oh, "Acousto-optic control of speckle contrast in multimode fibers with a cylindrical piezoelectric transducer oscillating in the radial direction," *Opt. Express* **17**(20), 17536–17546 (2009), <http://www.opticsinfobase.org/abstract.cfm?uri=oe-17-20-17536>.
17. L. Yuan, J. Yang, C. Guan, Q. Dai, and F. Tian, "Three-core fiber-based shape-sensing application," *Opt. Lett.* **33**(6), 578–580 (2008).

1. Introduction

Since the advent of a laser, laser beam shaping has been at the center of interests to both industry and academia, which requires delicate control of intensities and phase profiles of optical fields. One of the well established areas in beam shaping is homogenizing a Gaussian-like beam into a flat-top distribution for applications in lithography, material processing, and display [1]. Generating furthermore complex patterns has been a continuous issue for applications in more fundamental sciences to study light-matter interactions, and has been mainly developed by means of Fourier optics [2] such as diffraction by exotic apertures [3], deflection by MEMS mirror devices [4,5], and holography [6] to name a few.

Prior beam shaping arts have been traditionally based on bulk-optic systems, which restrict their potential applications in emerging research areas of nano- and micro-scale imaging and sensing. Fiber optics could be a strong candidate to miniaturize the beam shaping systems into the micro and sub-micro scale taking full advantage of its flexible guidance with built-in alignment. However, conventional circular-core fibers have provided only the Gaussian-like beam for both near and far fields leaving almost no room to further modify the beam characteristics. Since the late 1990s, there have been alternative optical waveguides based on micro air-silica structures [7], and the authors have also proposed a hollow optical fiber (HOF) that is composed of a central air hole, a high-index ring core, and silica cladding for applications in various photonic devices [8]. The central air hole in the HOF was found to have a significant effect on free-space light propagation, and the authors recently demonstrated an all-fiber hybrid structure to generate a rarely diffracting Bessel-like beam [9]. Despite successful adoption of the HOF in beam shaping, the beams were cylindrically symmetric about the propagation axis, and beam patterns with low-fold symmetry have not been realized in optical fibers.

There have been researches on polygonal-core fibers [10,11] that are in fact very similar to the stack-and-draw method used in micro air-silica structured fibers, but their primary aims were to simplify the preform fabrication in the early stage of fiber optics without further investigation on near- and far-field patterns. A preliminary study for unique beam shaping with an optical fiber was initiated by Tynes [12]; a triangular core suspended by a glass tube showed unique far-field patterns, which could be understood by his own quasi-ray-optic cavity-like model. Despite such unique beam shaping capabilities, the structure still suffered from interfacial defects and impurities, and further investigation has not been continued due to rapid growth of chemical vapor deposition in preform fabrication. Until nowadays, embedding polygonal-core structures along with micro holes into an optical fiber is still challenging.

Recently, the authors successfully developed a technique to embed a polygonal core into a cylindrical optical fiber with and without a central air hole [13]. Combining with the polygonal core, the central air hole generates various far-field patterns out of the fiber, which can be directly applied to all-fiber beam shaping. In this paper, we introduce a hollow triangular-core fiber (HTCF) as the simplest case to combine a triangular core with a central air hole, for the first time. Detailed fabrication processes and unique diffraction patterns are explained, which could not be achieved by conventional fibers. To understand the origin of unique evolution of the patterns, we also theoretically simulated propagation of the eigenmodes of the HTCF using Fourier optics to have a good agreement with experimental observations.

2. Embedding a hollow triangular core into a cylindrical optical fiber

The whole processes to fabricate a preform for the HTCF are schematically illustrated in Fig. 1(a) and more details on the fabrication can be found in [13]. Firstly, core layers composed of $\text{GeO}_2\text{-SiO}_2$ glass were deposited inside a silica substrate tube, Heraeus F300 [14] whose outer diameter (OD) and inner diameter (ID) are 25 and 19 mm, respectively, using modified chemical vapor deposition (MCVD). The tube was then partly collapsed to an OD of

19.8 mm and an ID of 11.4 mm for a central air hole. The cylindrical tube was polished to make a triangular cross section, which is also shown in Fig. 1(b); the maximum polishing depth was 1.7 mm. This triangular tube was then further collapsed in the MCVD lathe to a nearly circular shape with an OD of 14.6 mm and an ID of about 1 mm at a high temperature above the melting point of silica. During this high-temperature collapsing process, the middle of each side is pulled outward by the surface tension leaving the vertices of the tube intact. The GeO_2 doped ring also follows similar transformation to result in a triangular core with circular air hole in the center. The preform was then drawn to a fiber in optimized conditions to maintain the central hole in the fiber with proper He-gas pressure control. A cross section of the drawn HTCF is shown in Fig. 1(c) with an air-hole diameter of 18 μm , an equilateral-side length of 36 μm , and a cladding diameter of 200 μm . The ratio of the triangular core's side length to the air-hole diameter is about the square root of three. Attenuation of the drawn HTCF was measured as 14.2 and 65.2 dB/km at the wavelengths of 635 and 1550 nm, respectively. Relatively high loss was attributed to OH overtones. However, the fiber length used in the experiments was only a few centimeters, and the effect of fiber loss was negligible. Note that the time to fabricate the HTCF is comparable to that of the conventional optical fibers because the only additional process was shaping a triangular cross section using a conventional diamond saw.

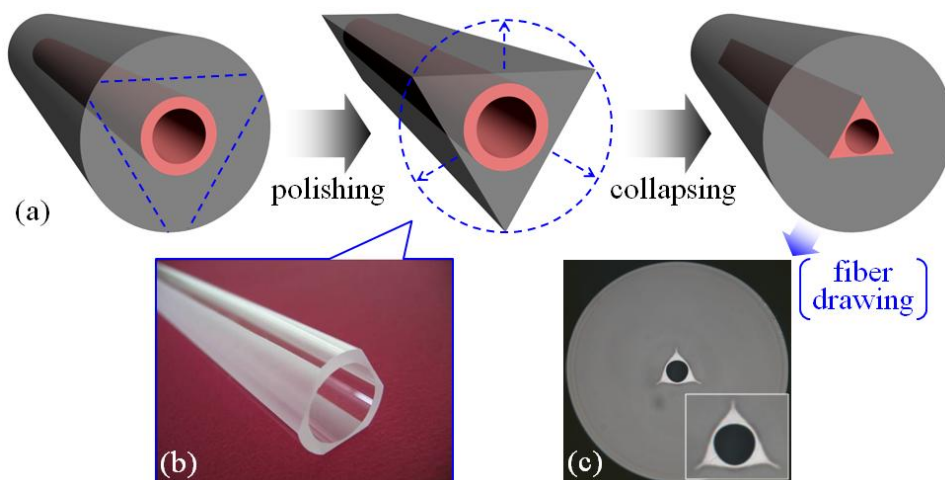


Fig. 1. (a) Schematic fabrication processes to make a preform for the HTCF: the MCVD, side-cutting and polishing, and collapsing. (b) A triangular tube after side polishing. (c) A cross section of the drawn HTCF.

3. Diffraction analysis and beam shaping by the HTCF

The near-field patterns of the HTCF are shown as a function of the incident-light wavelength λ in Fig. 2. The HTCF was cleaved at the right angle and various wavelengths were selected by using narrow band-pass interference filters and a tungsten-halogen lamp. For a shorter λ , many modes were overlapped over the whole cross section of the hollow triangular core. As λ increased, fewer modes are guided and the light intensity gradually spread toward the corners and expanded into the cladding.

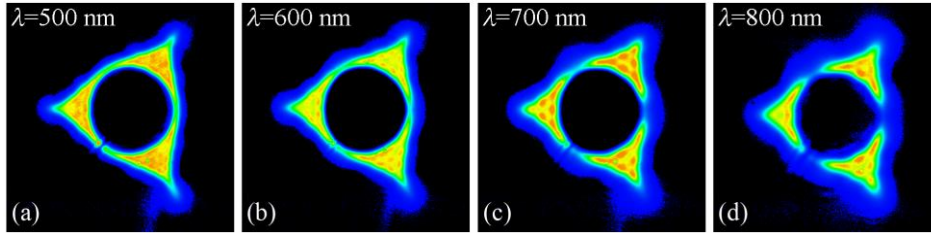


Fig. 2. Near-field patterns of the HTCF for various λ of (a) 500 nm, (b) 600 nm, (c) 700 nm, and (d) 800 nm.

The three-fold symmetry and the central air hole of the HTCF will generate totally new evolution of its diffraction patterns in comparison to conventional circular-core fibers. A laser diode (LD, $\lambda = 635$ nm) and a CCD camera were used to measure the beam patterns from the HTCF up to the axial length z of $750 \mu\text{m}$ with the interval Δz of $30 \mu\text{m}$ as schematically shown in Fig. 3. Note that light carried along a conventional single mode fiber (SMF) was efficiently coupled to the HTCF by an adiabatic mode conversion process that is similar to the case of the HOF [8,15]. When the HTCF is locally heated, for example by applying an electric arc in a fusion splicer, the central air hole collapses to a solid triangular core. When a modal intensity profile of the solid triangular core is designed to match that of the LP_{01} mode in the SMF, we can expect very low-loss coupling between the HTCF and the SMF. In the experiments, the lowest insertion loss by the adiabatic mode conversion was measured about 1 dB. The loss is mainly attributed to the mismatch in mode-field area between the solid triangular core of the collapsed HTCF and the circular core of the SMF. Unique evolution of the diffraction patterns out of the HTCF is categorized in Fig. 4 and the corresponding actual diffraction patterns are also shown in Fig. 5. Note that the intensity and the size of the patterns were normalized for fair comparison. The length of the HTCF can be reduced to a few millimeters with optimal adiabatic splicing with the SMF. In the experiments, we used the HTCF a few centimeter long. In this length scale, mode mixing caused by fiber vibrations in multimode fibers [16] is negligible due to the rigidity of the silica fiber. The far-field patterns from the HTCF were maintained stable against mechanical vibrations.

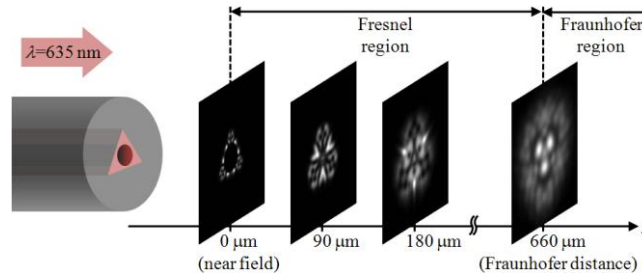


Fig. 3. Evolution of patterns from the near field to the far field for $\lambda = 635$ nm out of the HTCF

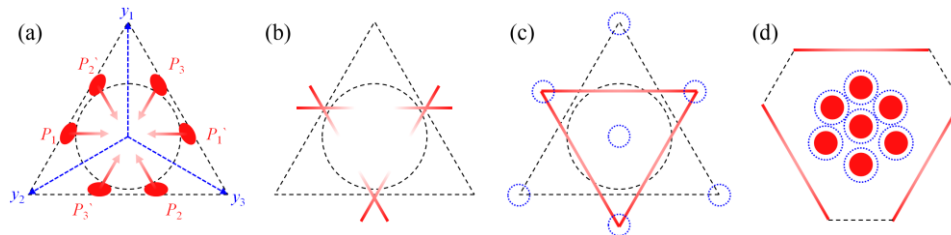


Fig. 4. Schematic description of diffraction evolution out of the HTCF from the near field to the far field.

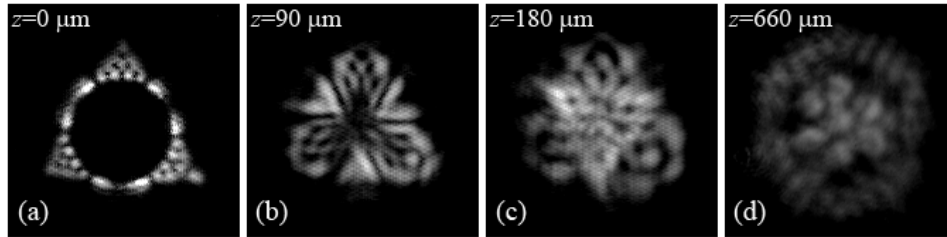


Fig. 5. Measured intensity patterns out of the HTCF at different axial positions for $\lambda = 635$ nm. (a) Near field, (b) 90 μm , (c) 180 μm , and (d) 660 μm and beyond.

At the near field, the intensity of the HTCF showed six extrema around the sides of the hollow triangular core as schematically shown in Fig. 4(a) and in its photograph in Fig. 5(a). The six extrema in the near-field pattern are denoted as $P_1, P_1', P_2, P_2', P_3,$ and P_3' in Fig. 4(a). As soon as the beam propagates along the axial direction, these initial extrema points were dragged into the center to form three lines $P_1-P_1', P_2-P_2',$ and P_3-P_3' , and each line was gradually driven outward from the center along its vertical blue y axis as in Fig. 4(a). As the axial distance increases, these lines merged together to form a shape of scissors at the middles of the triangle's sides as in Fig. 4(b). The corresponding measurement is shown in Fig. 5(b). As the beam further propagates, the continuously driven lines resulted in the Star of David as in Fig. 4(c) and the corresponding measurement is shown in Fig. 5(c). Until the axial distance reaches the Fraunhofer distance of ~ 660 μm , the corners and the center of the star indicated by the dashed blue circles in Fig. 4(c) packed together to form a hexagonal distribution as in Fig. 4(d). Corresponding measurement is shown in Fig. 5(d). Beyond this axial position, the beam showed Fraunhofer diffraction such that the shape did not change any longer. Note that this type of diffraction patterns with low-fold symmetry have not been realized in fiber optics even with multicore optical fibers [17], and the authors believe that this technique based on the central hole can open a new avenue of fiber-optic application for novel beam shaping.

4. Fourier-optic analysis for the guided modes in the HTCF

Drastic evolution of the diffraction patterns out of the HTCF in micro scale has never been reported, and it is very worthwhile to analyze its characteristics based on the intensity distribution of guided modes and their collective propagation in free space. To systematically analyze such unique diffraction evolution, we employed two theoretical electromagnetic wave analyses: 1) full vectorial finite difference frequency domain (FDFD) method with perfectly matched layer (PML) boundary conditions [18] to obtain guided modes in the HTCF for $\lambda = 635$ nm and 2) angular spectrum of plane waves (ASPW) for fast calculation of optical diffraction [2].

To simplify the modal calculation, we assume that the central air hole is a perfect circle, that the triangle is equilateral, and that their individual centers are overlapped on the fiber axis. The geometrical factors used in the simulations are same with the actual HTCF: a central air-hole diameter of 18 μm , the equilateral hollow triangular core with its side length of 36 μm . The mode calculation was rigorously carried out, and forty-six guided modes were obtained for $\lambda = 635$ nm. The guided modes could be divided into two categories: 1) thirty-six modes which can be grouped by polarization degeneracy with the three-fold nature and 2) the next ten higher-order hybrid modes which cannot be grouped. Representative modes of the first category are shown in Fig. 6 which shows only modes with intensity distributions confined in the top vertex of the hollow triangular core. Note that the modes whose intensities are confined to other two vertices have the same effective refractive indices by the symmetry. After these thirty-six modes, we could further identify ten higher-order modes whose modal intensities are shown in Fig. 7. Note that these modes fill the almost all the area of the hollow triangular core and that they share neither polarization degeneracy nor the three-fold nature contrary to the lower-order modes. This type of different polarization degeneracy in the

higher-order modes is quite common in waveguide analysis. For example in weakly guiding cylindrical waveguides, the unique nature of radial polarization in TE, TM, and HE modes is no longer observed in the higher-order hybrid LP_m modes. More detailed analyses for these unique modal properties are being pursued by the authors and will be published in a separate paper.

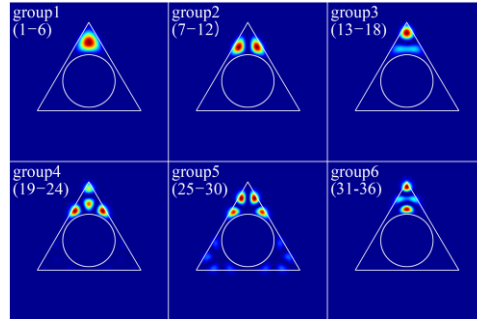


Fig. 6. Representative modes (whose intensities are mainly confined within the top vertex of the hollow triangular core) for each group for $\lambda = 635$ nm.

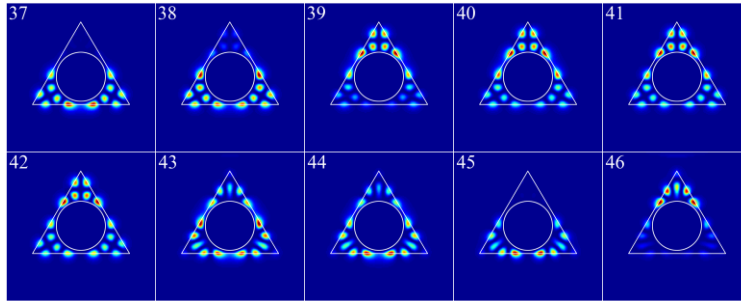


Fig. 7. The next ten higher-order modes which cannot be grouped.

Having identified the guided modes, we then carried out the ASPW calculation for the propagation of the composite intensity distributions composed of those guided modes shown in Figs. 6 and 7. It would be a very difficult task to precisely predict a diffracted beam pattern from composite intensity distributions made by the multiple modes because the phase among the neighboring modes changes in a random manner to generate a speckle pattern. As a starting point of diffraction pattern calculation, we tried both vectorial summations of the electric fields and scalar summations of the modal intensities to simulate the actual near-field pattern of the HTCF as shown in Fig. 5(a) as close as possible. After trial and error, we found that the near-field pattern can be best fit by scalar summation of the normalized intensity of the modes,

$$I_{z=0} \propto \sum_{m=1}^{46} |E_m(x, y)|^2. \quad (1)$$

Contribution from the first thirty-six modes was found to be significantly less than that of the next ten higher-order modes, whose causes are being investigated by the authors. Therefore, Eq. (1) can be approximated as

$$I_{z=0} \propto \sum_{m=37}^{46} |E_m(x, y)|^2. \quad (2)$$

For far-field visualization of a certain mode, the ASPW propagation operator can be applied to its complex field at the near field [2],

$$\mathcal{P}_z^{\text{ASPW}} E(x, y) = \mathcal{F}^{-1} \left(\exp \left\{ 2\pi i z \left[\left(n / \lambda \right)^2 - k_x^2 - k_y^2 \right]^{1/2} \right\} \mathcal{F} E(x, y) \right), \quad (3)$$

where n is a refractive index of a surrounding medium, k is a wave number, and \mathcal{F} and \mathcal{F}^{-1} are the Fourier and its inverse transform operators, respectively;

$$\mathcal{F} E(x, y) = \iint_{-\infty}^{\infty} dx dy \exp \left[-2\pi i (xk_x + yk_y) \right] E(x, y), \quad (4)$$

$$\mathcal{F}^{-1} E(k_x, k_y) = \iint_{-\infty}^{\infty} dk_x dk_y \exp \left[2\pi i (xk_x + yk_y) \right] E(k_x, k_y). \quad (5)$$

For each axial position z , the intensities of the propagated modes were summed again, i.e.

$$I_{z>0} \propto \sum_{m=37}^{46} \left| \mathcal{P}_z^{\text{ASPW}} E_m(x, y) \right|^2, \quad (6)$$

and the simulation results are shown in Fig. 8 showing evolution of the diffraction patterns along the axial position. The simulation results in Figs. 8(a)~(c) do agree well with the experimental measurements in Figs. 5(a)~(c) in terms of symmetry and intensity contrast, showing characteristic evolution of spatial symmetry as described in Fig. 4. The patterns in Figs. 5(d) and 8(d) show a notable difference in the intensity contrast especially among the central seven bright spots. Although brightness of these spots in Fig. 8(d) is different, their symmetric distribution in a hexagon indeed matches to that of Fig. 5(d). We could confirm that the simulation also showed Fraunhofer diffraction beyond 660- μm propagation distance. Subtle discrepancy between Figs. 5 and 8 might be attributed to the exclusion of lower-order modes' influence and the structural imperfection of the fabricated HTCF as well as numerical errors in simulations.

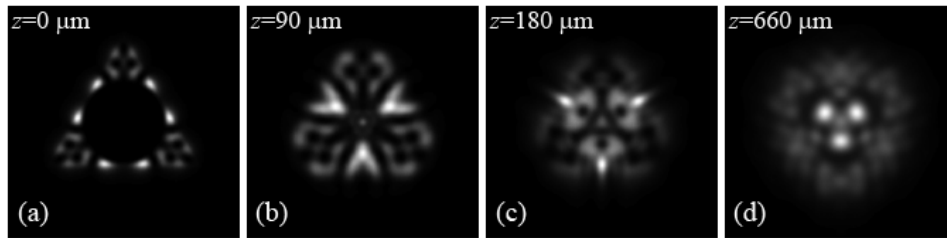


Fig. 8. Simulation of diffraction evolution based on Eq. (6) for the propagation distances of (a) 0, the near field pattern, (b) 90 μm , (c) 180 μm , and (d) 660 μm , the Fraunhofer diffraction pattern.

In this simulation, we could confirm that the polygonal core embedded in a cylindrical optical fiber can provide very rich diversity of diffraction patterns, which can be controlled by the geometry of the core and the central air hole. This technique can provide a new degree of freedom in fiber-optic design for laser beam shaping applications. Despite good agreement between simulations and measurements, the authors do find that the assumption behind the simulations, decoupled modes during propagation, should be further investigated in detail. Rigorous theoretical analyses for the complex multimode propagation are beyond the scope of this paper, and remains as a future work being pursued by the authors.

5. Conclusion

In conclusion, we successfully developed the novel fabrication processes to embed a hollow triangular core in cylindrical optical fibers by inverting the symmetry of the triangular preform inside out in the optical fiber during high-temperature collapsing, and the HTCF was successfully fabricated. Unique diffraction pattern evolution out of the cleaved HTCF were observed using an LD of $\lambda = 635 \text{ nm}$ and a CCD camera, where the intensity extrema showed

a systematic change from the near-field pattern to Fraunhofer diffraction. For systematic analyses, forty-six guided modes were found by the FDFD method with PML boundary condition. It was found that the scalar summation of the ten higher-order modes' intensities by propagation of the ASPW resulted in evolution of the diffraction patterns with a good agreement with experimental measurements. The triangular core with the central hole in an optical fiber was found to give high potential in all-fiber beam shaping, which can be readily applied in novel nano- and micro-pattern generation.

Acknowledgments

This work was supported in part by the Brain Korea 21 Project and in part by the NRF grant funded by the MEST (Nos. 2010-0018442, 2009-00479 EC-FP7/2007-2013 219299 GOSPEL, R15-2004-024-00000-0, and 2009-352-C00042).